Coupling and splitting of the plasmon modes in a superlattice with complex defect structures



2004 J. Phys.: Condens. Matter 16 1075

(http://iopscience.iop.org/0953-8984/16/7/007)

INSTITUTE OF PHYSICS PUBLISHING JOURNAL OF PHYSICS: CONDENSED MATTER

J. Phys.: Condens. Matter **16** (2004) 1075–1086 PII: S0953-8984(04)71984-0

# Coupling and splitting of the plasmon modes in a superlattice with complex defect structures

**Xi-Li Zhang**[1], **Ben-Yuan Gu**[1,2] **and Xue-Hua Wang**[1]

[1] Institute of Physics, Chinese Academy of Sciences, PO Box 603, Beijing 100080, People's Republic of China
[2] CCAST (World Laboratory), PO Box 8730, Beijing 100080, People's Republic of China

E-mail: c412-1@aphy.iphy.ac.cn (Xi-Li Zhang)

Received 14 November 2003
Published 6 February 2004
Online at stacks.iop.org/JPhysCM/16/1075 (DOI: 10.1088/0953-8984/16/7/007)

**Abstract**

We study the properties of the localized interface plasmon modes (IPMs) arising from coupling and splitting of the plasmon eigenstates in two semi-infinite superlattices containing complex defect structures. Two kinds of defect structure are considered: one is a single quantum well, i.e., a barrier–well–barrier structure; the other is a well–barrier–well structure. The influences of the constitution of the defect structures, as well as the physical and geometric parameters of the superlattices on the characteristics of the localized IPMs are investigated in detail. The numerical results show that the localized modes exhibit peculiar features; the complexity of the dispersion of IPMs is essentially associated with the coupling of the interwell regions in the defect structure, and the barrier and well layers play different roles in the features of the localized IPMs. We also present a comparison of the dispersions of the localized IPMs between these two types of defect structure and give a physical picture to explain these results.

## 1. Introduction

In the past few decades, there has been continuous effort in studying collective excitations of the two-dimensional layered electron gas (2DLEG) in semiconductor superlattices, especially following the developments in the techniques of superlattice growth and the fabrication of microstructures, such as molecular-beam epitaxy and metal–organochemical vapour deposition. The dispersion relation of the bulk plasmons of the 2DLEG in perfect superlattices has been intensively analysed theoretically on the basis of both macroscopic and microscopic methods [1–5]. The plasmon spectrum has also been measured by means of Raman scattering experiments [2, 6]. For an ideal superlattice consisting of a periodic array of doped quantum wells, the two-dimensional plasmon excitations of the individual quantum well are coupled together by the long-range Coulomb force; the bulk plasmon modes have been found to form

  

a band structure which strongly depends on the periodicity of the superlattice. However, when such periodicity is broken, localized states occur, which holds true for electrons [7–11], acoustic phonons [12–14], and interface optical phonons [15–17] in aperiodic superlattices or semi-infinite superlattices. In the case of the semi-infinite superlattices, various authors have explored the properties of the surface plasmon modes at the interface between a semi-infinite superlattice and an adjoining bulk material when the dielectric constants of the two materials are different [18, 19]. The occurrence of surface plasmon modes significantly relies on the ratio of the dielectric constants of the two materials. The localized interface plasmon modes (IPMs) in a system composed of two semi-infinite semiconductor superlattices separated by a space of $d$ have also been explored [20]. Two branches consisting of higher-energy and lower-energy IPMs are found arising from symmetric or antisymmetric linear combinations of plasmon eigenstates of the prototype perfect superlattices.

The present work is inspired by the above-mentioned research work. We have studied the localized interface optical phonon modes in the previous research [21, 22]. In this paper, we extend our foregoing work to studies of the properties of localized IPMs in a system consisting of a complex defect structure, such as structures containing $N$ quantum wells, each sandwiched by two semi-infinite semiconductor superlattices. By solving Maxwell's equations and using the linear response theory, we derive general formulae suitable for calculating the dispersion relation of the localized IPMs in the system considered here. We discuss two special structures: one is the defect structure composed of a single quantum well, i.e., the barrier–well–barrier (BWB) structure; the other is the well–barrier–well (WBW) defect structure. We numerically investigate the effects of the coupling between two semi-infinite superlattices, as well as the coupling between the superlattice and the defect structure, on the plasmon bulk bands and localized IPMs. We find that the present structures exhibit peculiar and interesting properties of the localized IPMs: the maximal number of localized IPMs is different for BWB and WBW defect structures, and the barrier and well layers in defect structures play different roles in the features of the dispersions of the localized IPMs. The coupling of the plasmon excitations of the superlattices results in the creation of unique localized IPMs. We also present a comparison of the dispersion of the localized IPMs between the BWB and WBW defect structures and give a simple physical picture to explain these results.

This paper is organized as follows. In section 2, we present a brief description of the model and the necessary formulae used in the calculations. The numerical results together with an analysis are given in section 3. Finally, we summarize our main findings of this work in section 4.

## 2. Model and formulae

We consider a system depicted in figure 1, which is composed of a complex defect structure sandwiched by two semi-infinite superlattices. The left-hand-side superlattice (labelled superlattice I) has a period of $b$, and the uniformly doped electron density is $n_1$. However, the superlattice on the right-hand side (labelled superlattice III) has a different period of $a$, and the doped electron density is $n_3$. The defect structure (defect II) consists of a finite array of $N$ quantum wells, each of which has a specific period of $d_l$ ($l = 1, \ldots, N$) and the doped electron density is $n_{\mathrm{II},l}$. The average dielectric constants of superlattice I, superlattice III, and defect II are $\epsilon_1$, $\epsilon_3$, and $\epsilon_2$, respectively. Besides this, the growth direction of the superlattices is along the $z$ direction; and every layer in the superlattices or defect structures is located on the $xy$ plane. The origin of the coordinates is set at the rightmost edge of the left semi-infinite superlattice I, as seen in figure 1. Here, we assume that the quantum well is so thin that the 2DLEG is formed and arrayed separated by a spacing distance. This model has been widely adopted in the calculations by many authors [1–5, 18–20, 23].

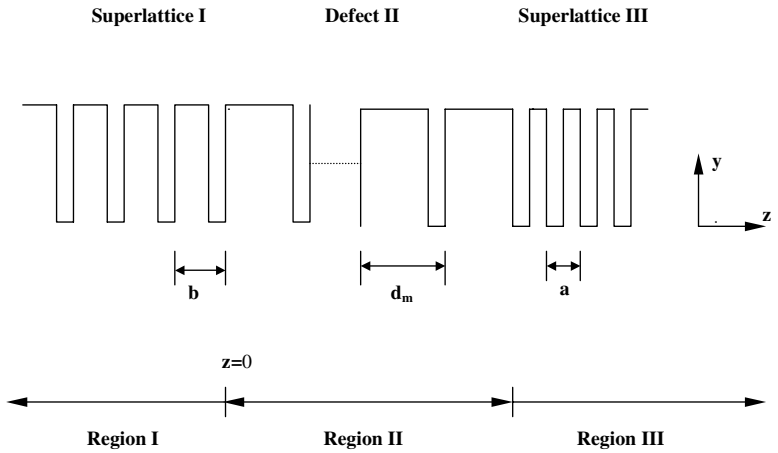


**Figure 1.** A schematic representation of two coupled semi-infinite superlattices separated by a complicated defect structure. The periods of superlattices I (on the left-hand side) and III (on the right-hand side) are $b$ and $a$, respectively. The defect structure standing between them consists of $N$ quantum wells, each of which has the period of $d_l$ $(0 \leqslant l \leqslant N)$.

In view of the success of Maxwell's equations coupled to the density response of two-dimensional electron sheets in treating localized and surface plasmon excitations, in this paper we adopt them to investigate the localized IPMs. The following boundary conditions must be satisfied: the tangential component of the electric field is continuous and the normal component of the displacement vector is discontinuous, by $4\pi\rho$, across each interface. Thus, we can derive the equations for determining the dispersion relation of the localized IPMs. For a p-polarized electromagnetic wave, from Maxwell's equations

$$\nabla \times \mathbf{H} = \frac{\partial \mathbf{D}}{\partial t} = -\mathrm{i}\omega\epsilon_0\epsilon_r\mathbf{E} \tag{1}$$

and

$$(\nabla \times \mathbf{E})_x = \left(-\frac{\partial \mathbf{B}}{\partial t}\right)_x = \mathrm{i}\omega\mu_0\mu_r H_x, \tag{2}$$

we can derive the equation satisfied by $H_x$:

$$\left[\frac{\partial^2}{\partial y^2} + \frac{\partial^2}{\partial z^2} + \frac{\omega^2}{c^2}\epsilon_r\mu_r\right]H_x = 0. \tag{3}$$

So the formal solution for $H_x$ is

$$H_x = (A\mathrm{e}^{-\mathrm{i}k_z z} + B\mathrm{e}^{\mathrm{i}k_z z})\mathrm{e}^{\mathrm{i}k_y y}. \tag{4}$$

Substituting equation (4) into (1), the components of the electric field $E_y$ and $E_z$ can be easily calculated. In terms of the Bloch theorem, the periodicity of the superlattice gives rise to Bloch-type propagation wave solutions. Due to the translation invariance of the system structures considered here in the $xy$ plane, therefore, only two components of wavevectors are necessary in the solutions. Consequently, the non-zero components of the electric fields in the three regions can be written as follows [20, 23, 24]:

$$E_y = \begin{cases} [E^+_{1,0}\mathrm{e}^{-\mathrm{i}\beta_1(z-z_m^{(1)})} + E^-_{1,0}\mathrm{e}^{\mathrm{i}\beta_1(z-z_m^{(1)})}]\mathrm{e}^{\mathrm{i}q_z^{(1)}(m-1)b}, & -b \leqslant z - z_m^{(1)} \leqslant 0 \text{ (region I)}, \\ [E^+_{2,l}\mathrm{e}^{\mathrm{i}\beta_2(z-z_l^{(2)})} + E^-_{2,l}\mathrm{e}^{-\mathrm{i}\beta_2(z-z_l^{(2)})}], & 0 \leqslant z - z_l^{(2)} \leqslant d_l \text{ (region II)}, \\ [E^+_{3,0}\mathrm{e}^{\mathrm{i}\beta_3(z-z_m^{(3)})} + E^-_{3,0}\mathrm{e}^{-\mathrm{i}\beta_3(z-z_m^{(3)})}]\mathrm{e}^{\mathrm{i}q_z^{(3)}(m-1)a}, & 0 \leqslant z - z_m^{(3)} \leqslant a \text{ (region III)}, \end{cases} \tag{5}$$

$$E_z = \begin{cases} q\beta_1^{-1}[E_{1,0}^{+}\mathrm{e}^{-\mathrm{i}\beta_1(z-z_m^{(1)})} - E_{1,0}^{-}\mathrm{e}^{\mathrm{i}\beta_1(z-z_m^{(1)})}]\mathrm{e}^{\mathrm{i}q_z^{(1)}(m-1)b}, \\ \quad -b \leqslant z - z_m^{(1)} \leqslant 0 \text{ (region I)}, \\ -q\beta_2^{-1}[E_{2,l}^{+}\mathrm{e}^{\mathrm{i}\beta_2(z-z_l^{(2)})} - E_{2,l}^{-}\mathrm{e}^{-\mathrm{i}\beta_2(z-z_l^{(2)})}], \\ \quad 0 \leqslant z - z_l^{(2)} \leqslant d_l \text{ (region II)}, \\ -q\beta_3^{-1}[E_{3,0}^{+}\mathrm{e}^{\mathrm{i}\beta_3(z-z_m^{(3)})} - E_{3,0}^{-}\mathrm{e}^{-\mathrm{i}\beta_3(z-z_m^{(3)})}]\mathrm{e}^{\mathrm{i}q_z^{(3)}(m-1)a}, \\ \quad 0 \leqslant z - z_m^{(3)} \leqslant a \text{ (region III)}. \end{cases} \tag{6}$$

Of course, the harmonic time factor $\mathrm{e}^{\mathrm{i}(qy-\omega t)}$ should be attached to all the above expressions. Here $\mathbf{q} = (q, q_z^{(n)})$ stands for the two components of the plasmon wavevectors parallel and perpendicular to the interface, and $\beta_n$ is related to the parallel component $q$ by the relationship $\beta_n^2 = \epsilon_n\omega^2/c^2 - q^2$, where $n$ denotes the specific regions I, II, and III. $z_l^{(2)} = \sum_{i=1}^{l} d_i$ and $z_m^{(3)} = \sum_{i=1}^{N} d_i + ma$ denote the coordinates of the left-hand-side beginning of the $l$th layer in defect II and the $m$th layer in superlattice III, respectively. For a symmetric structure, $z_m^{(1)} = -mb$ defines the coordinate of the right-hand-side beginning of the $m$th layer in superlattice I, where $m$ is taken to be a positive integer.

For the localized IPMs, the Bloch wavenumbers $q_z^{(1)}$ and $q_z^{(3)}$ for superlattices I and III should take complex values in the forms

$$q_z^{(1)} = \frac{k\pi}{b} + \mathrm{i}q_0^{(1)} \qquad (q_0^{(1)} > 0, \quad k = 0, 1, 2, \ldots), \tag{7a}$$

$$q_z^{(3)} = \frac{k'\pi}{a} + \mathrm{i}q_0^{(3)} \qquad (q_0^{(3)} > 0, \quad k' = 0, 1, 2, \ldots). \tag{7b}$$

With the use of the continuity of the $E_y$ and the discontinuity of the $E_z$ at every interface, the dispersion equation is determined by

$$\cosh(\mathrm{i}q_z^{(1)}b) - \cosh(qb) = \tfrac{1}{2}r_1\sinh(qb), \tag{8a}$$

$$\cosh(\mathrm{i}q_z^{(3)}a) - \cosh(qa) = \tfrac{1}{2}r_3\sinh(qa), \tag{8b}$$

$$A_{\mathrm{II},1}[T(2,1)A_{\mathrm{II},N} + T(2,2)] - T(1,1)A_{\mathrm{II},N} - T(1,2) = 0, \tag{8c}$$

where $r_1$ and $r_3$ are given respectively by

$$r_1 = -\frac{4\pi(e^*)^2 n_1 q}{\epsilon_1 m^*\omega^2},$$

$$r_3 = -\frac{4\pi(e^*)^2 n_3 q}{\epsilon_3 m^*\omega^2},$$

where $e^*$ and $m^*$ are the charge and effective mass of the electrons in the quantum well. Here, the interaction of the plasmon modes with the electromagnetic modes is not considered. $A_{\mathrm{II},1}$ represents the amplitude ratio $E_{2,1}^{+}/E_{2,1}^{-}$ of the first layer in defect region II, $A_{\mathrm{II},N}$ being the amplitude ratio $E_{2,N}^{+}/E_{2,N}^{-}$ of the $N$th layer in defect region II. Their particular expressions are

$$A_{\mathrm{II},1} = \frac{\frac{\epsilon_2}{\epsilon_1}\sinh(qb) - [\mathrm{e}^{-\mathrm{i}q_z^{(1)}b} - \cosh(qb)]}{\frac{\epsilon_2}{\epsilon_1}\sinh(qb) + [\mathrm{e}^{-\mathrm{i}q_z^{(1)}b} - \cosh(qb)]}$$

and

$$A_{\mathrm{II},N} = \frac{\frac{\epsilon_2}{\epsilon_3}\sinh(qa) + [\mathrm{e}^{-\mathrm{i}q_z^{(3)}a} - \cosh(qa)]}{\frac{\epsilon_2}{\epsilon_3}\sinh(qa) - [\mathrm{e}^{-\mathrm{i}q_z^{(3)}a} - \cosh(qa)]}\mathrm{e}^{2qd_N}.$$

The matrix $T$ describes the propagation of the amplitude factor from the first to the $N$th quantum well in defect region II, and it is given by

$$T = \prod_{l=1}^{N-1} P^{-1}(q, d_l) Q(r_{\mathrm{II},l}), \tag{9}$$

where

$$P(q, z) = \begin{pmatrix} \mathrm{e}^{-qz} & \mathrm{e}^{qz} \\ \mathrm{e}^{-qz} & -\mathrm{e}^{qz} \end{pmatrix},$$

and

$$Q(r) = \begin{pmatrix} 1 & 1 \\ r+1 & r-1 \end{pmatrix}.$$

$r_{\mathrm{II},l}$ has an analogous form to $r_1$ (or $r_3$) except for the replacement of $\epsilon_1$ and $n_1$ respectively by $\epsilon_2$ and $n_{\mathrm{II},l}$.

Note that equations (8$a$) and (8$b$) together describe the dispersion relation of the bulk plasmons for perfect and infinite superlattices I and III when $q_z^{(1)}$ and $q_z^{(3)}$ are real numbers. The plasmon occurs only for the condition $|\cosh(\mathrm{i}q_z^{(1)}b)| \leqslant 1$ or $|\cosh(\mathrm{i}q_z^{(3)}a)| \leqslant 1$, which gives the bulk plasmon band. For the localized IPMs, the parallel wavevector should be complex. Generally speaking, the localized IPMs in the infinite superlattices with any defect structures are determined by equations (8$a$)–(8$c$).

## 3. Results and discussion

### *3.1. BWB defect structure*

We now consider a case where the defect structure is composed of a single quantum well, i.e., a barrier–well–barrier (BWB) structure. The widths of the left and right barriers are $d_1$ and $d_2$, respectively; the electron density in the well layer is $n_{\mathrm{II},1}$. Equation (8$c$) can then be simplified to

$$A_{\mathrm{II},1}\mathrm{e}^{-qd_1}\left[1 - \frac{r_{\mathrm{II},1}}{2}(1 + A_{\mathrm{II},2})\right] - \mathrm{e}^{qd_1}\left[A_{\mathrm{II},2} + \frac{r_{\mathrm{II},1}}{2}(1 + A_{\mathrm{II},2})\right] = 0. \tag{10}$$

The dispersion relations of the localized plasmon modes are numerically determined by equation (10) and equations (8$a$), (8$b$). In the following calculations, all the frequencies are measured in units of the eigenfrequency $\omega_0$ associated with superlattice III, which is given by

$$\omega_0 = \left[\frac{4\pi(n_3/a)(e^*)^2}{m^*\epsilon_3}\right]^{1/2}. \tag{11}$$

The electron density and the period involved are scaled by their relative values with respect to those in superlattice III. We also assume that the dielectric constants of the materials in regions I, II, and III are identical, i.e., $\epsilon_1 = \epsilon_2 = \epsilon_3$.

We illustrate the frequency spectrum of the localized IPMs as a function of the transverse wavenumber $q$ in figure 2. Here, superlattices I and III possess the same period $a = b$ and the same doped electron density $n_1 = n_3$. The electron density $n_{\mathrm{II},1}$ in the quantum well is chosen as $n_{\mathrm{II},1}/n_3 = 0.5$. The widths of the right and left barriers of the quantum well in the defect structure are kept identical, as $0.1a$, $0.35a$, $0.5a$, and $0.7a$, and the spectra of the localized IPMs correspond to figures 2(a)–(d), respectively. The shaded areas confined by two dash–dotted curves with $\cosh \mathrm{i}q_z^{(1)}b = -1$ and 1 indicate the bulk plasmon bands, which correspond to the continuum of the bulk plasmons for the isolated superlattices. It

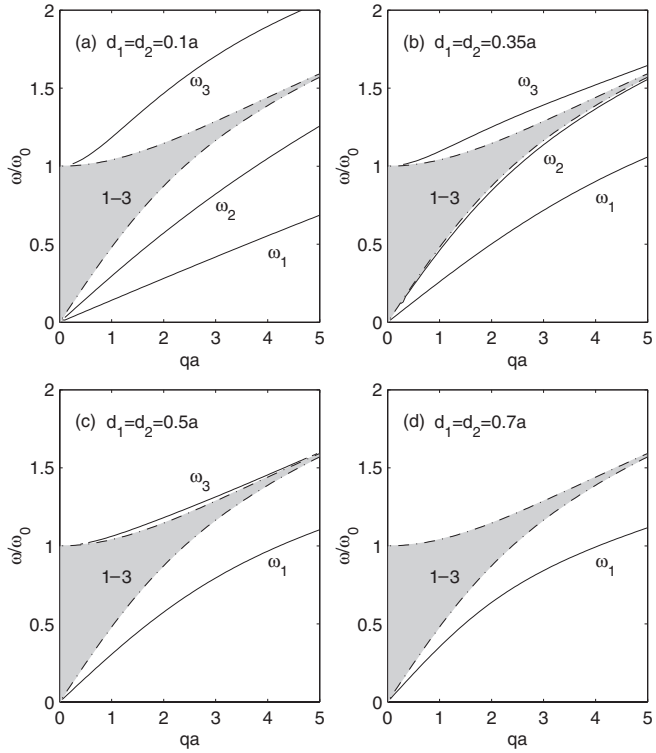


**Figure 2.** The dispersion spectrum of the localized IPMs as a function of the transverse wavenumber $q$ in the two semi-infinite superlattices separated by a BWB defect structure. Here, we set $a = b$, $n_1 = n_3$, and $n_{\mathrm{II},1}/n_3 = 0.5$. The right and left barrier widths are kept identical, as $0.1a$, $0.35a$, $0.5a$, and $0.7a$, and their localized IPMs correspond to (a)–(d), respectively. The shaded areas between two dash–dotted curves with $\cosh \mathrm{i}q_z^{(1)}b = -1$ and $\cosh \mathrm{i}q_z^{(1)}b = 1$ represent the bulk plasmon bands for the isolated superlattices I and III. The solid curves lying outside the bands are the localized IPMs.

should be emphasized that the bulk plasmon band is determined only by the periodic structure of the superlattices and the transverse wavenumber $q$, independently of the defect structure, as stated above from equations (8*a*) and (8*b*). Since superlattices I and III are completely identical, their bulk plasmon bulks overlap with each other. With the increase of the transverse wavevector $q$, the upper and lower band edges of the bulk plasmon modes approach closer and finally become degenerate at the boundary of the first Brillouin zone of the superlattices. It is clearly seen in figure 2(a) that three localized IPMs appear outside the bulk plasmon band: one is a higher-energy mode (marked as mode $\omega_3$) lying above the bulk plasmon band; the others are two lower-energy modes (marked as mode $\omega_1$ and $\omega_2$) lying below the bulk plasmon band. Besides these two conventional modes $\omega_1$ and $\omega_3$ corresponding to symmetric or antisymmetric combinations of plasmon eigenstates of the individual superlattices I and III, as discussed in [20], a new localized IPM $\omega_2$ is created. We also find that mode $\omega_2$ is much more sensitive to the variation of the parameters of the defect region. In the long-wavelength limit, the frequency of the modes $\omega_1$ and $\omega_2$ approaches zero when $q \to 0$, while the frequency of the mode $\omega_3$ approaches 1. On increasing $q$, the frequencies of three modes are increased. An interesting thing is that on increasing the width of $d_1$ and $d_2$ from $0.1a$ to $0.35a$, the mode $\omega_3$ shifts rapidly downward and approaches the upper band edge of the continuum of the bulk

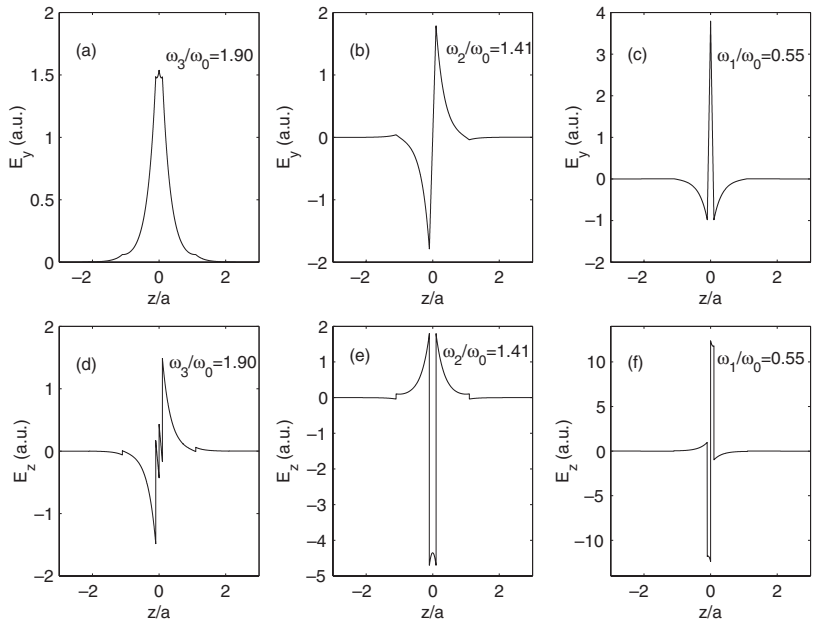


**Figure 3.** Distributions of the electric field for the localized IPMs calculated in figure 2(a). Parts (a) ((b), (c)) and (d) ((e), (f)) correspond to the tangential component $E_y$ and the normal component $E_z$ of the electric field, respectively, for the mode $\omega_3$ ($\omega_2$, $\omega_1$) with the frequency 1.90 (1.41, 0.55) in units of $\omega_0$. $\omega_0$ is the eigenfrequency associated with superlattice III.

plasmons; however, $\omega_2$ is rapidly shifted upward and approaches the lower band edge of the continuum of the bulk plasmons, as seen in figures 2(a) and (b). Further increasing the width of $d_1$ and $d_2$ to $0.5a$, the mode $\omega_2$ is merged into the continuum of the bulk plasmons; only two modes $\omega_1$ and $\omega_3$ survive, as seen in figure 2(c). When the widths $d_1$ and $d_2$ are equal to $0.7a$, the mode $\omega_3$ is also merged into the continuum of the bulk plasmons and only one mode $\omega_1$ is found, as shown in figure 2(d). The mode $\omega_1$ exhibits a weak dependence on the change of the widths $d_1$ and $d_2$ in the case of $d_1 = d_2$. The more sensitive dependence of the mode $\omega_2$ on the widths $d_1$ and $d_2$ when they are identical reveals the fact that this new localized IPM originates from the coupling of the defect structure and the superlattices; this coupling in turn leads to the splitting of the plasmon states and the creation of a new localized IPM.

To further reveal nature of the localized IPMs, we map out the distribution of the electric fields of the localized IPMs displayed in figure 2(a). Figures 3(a) ((b), (c)) and 3(d) ((e), (f)) correspond to the tangential component $E_y$ and the normal component $E_z$ of the electric fields for the mode $\omega_3$ ($\omega_2$, $\omega_1$) calculated in figure 2(a), with the frequency $\omega_3 = 1.90\omega_0$ ($\omega_2 = 1.41\omega_0$, $\omega_1 = 0.55\omega_0$). It is evident from figure 3 that the field distribution exhibits a certain symmetry or antisymmetry with respect to the central plane of the defect structures, and the symmetry of $E_y$ is always inverse to that of $E_z$ for these three modes. The symmetry of $E_y$ (or $E_z$) of the mode $\omega_2$ is opposite to that of the modes $\omega_1$ and $\omega_3$. Moreover, these modes are highly localized in the vicinity of the defect region, and they rapidly decay to zero, as demonstrated in figure 3. The continuity of $E_y$ and the discontinuity of $E_z$ at the interfaces are also obviously observed on comparing figures 3(a) ((b), (c)) with figures 3(d) ((e), (f)).

We now discuss the influence of the different widths ($d_1 \neq d_2$) of the constituent layers of the defect structure on the localized IPMs—different from that for the above sample with $d_1 = d_2$. We fixed the width $d_1$ of the left barrier of the quantum well to $0.1a$, but the width

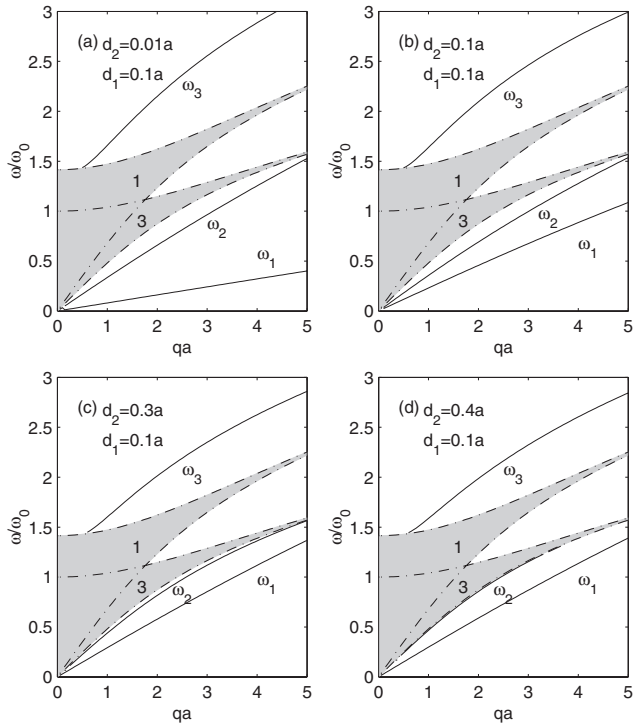


**Figure 4.** The influence of the width of the constituent layers of the defect structure on the localized IPMs in the same structure as in figure 2. We assume the width of the left barrier $d_1$ of the quantum well to be $0.1a$, but the width of the right barrier $d_2$ changes from $0.01a$, $0.1a$, $0.3a$, to $0.4a$. The corresponding numerical results are shown in (a)–(d). Other parameters are chosen as $n_1/n_3 = 2$, $n_{\mathrm{II},1}/n_3 = 2$, and $a = b$. The explanation of the curve styles is the same as for figure 2.

$d_2$ of the right barrier $d_2$ is changed from $0.01a$ to $0.1a$, $0.3a$, and $0.4a$. The corresponding numerical results are shown in figures 4(a)–(d), respectively. Other parameters are chosen as $n_1/n_3 = 2$, $n_{\mathrm{II},1}/n_3 = 2$, and $a = b$. It is clearly seen that there are two bulk plasmon bands: the upper one labelled as 1 corresponds to the continuum of the bulk plasmons in superlattice I; the lower one labelled as 3 corresponds to the continuum of the bulk plasmon modes in superlattice III. Compared with figure 2, the bulk plasmon bands 1 and 3 are separated from each other when $qa > 1.80$ due to the different electron densities in superlattices I and III. The mode $\omega_3$ occurs only when the parallel wavenumber $q$ is larger than a certain value depending on the ratio $n_1/n_3$. However, the modes $\omega_1$ and $\omega_2$ span the whole Brillouin zone, regardless of the electron density ratio $n_1/n_3$. In the long-wavelength limit, both $\omega_1$ and $\omega_2$ approach zero when $qa \to 0$; in contrast, $\omega_3$ approaches a finite frequency and it appears only when $qa$ is larger than a certain value. With the increase of $d_2$, mode $\omega_2$ rapidly approaches the lower band edge of continuum 3 of the bulk plasmons and, when $d_2 > 0.4a$, the mode $\omega_2$ is merged into continuum 3 and disappears completely, as seen in figure 4(d). By contrast, both modes $\omega_1$ and $\omega_3$ exhibit weak dependence on $d_2$. We conclude that the nature of mode $\omega_2$ is entirely different to that of modes $\omega_1$ and $\omega_3$. The mode $\omega_2$ stems from the effect of coupling among the superlattices and the defect structures.

We consider a special structure which is developed from the minor modification of the above-addressed sample in figure 4; we set $d_1 = a$ and all the other parameters remain unchanged from those of figure 4. In this case, the system can be regarded as two semi-infinite

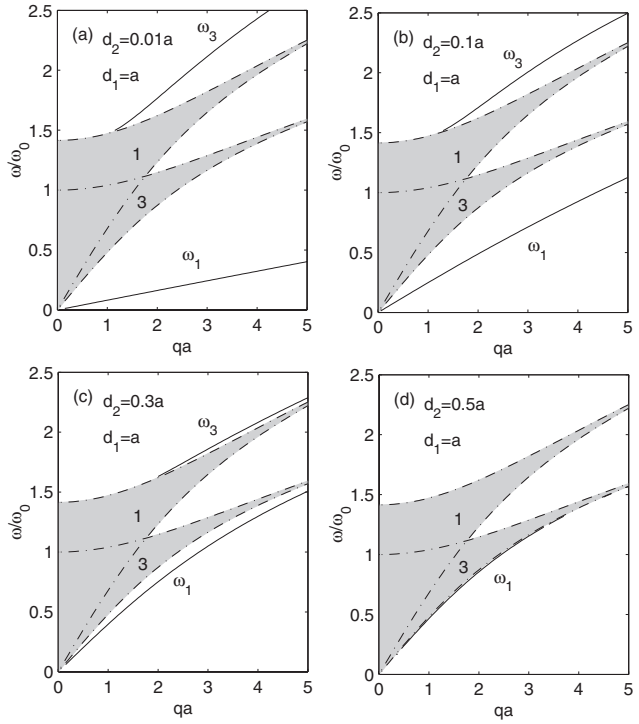


**Figure 5.** As figure 4 except for a change of the width $d_1$, i.e., $d_1 = a$. Parts (a)–(d) correspond to different widths $d_2$: $0.01a$, $0.1a$, $0.3a$, and $0.5a$, respectively. The explanation of the curve styles is the same as for figure 2.

superlattices separated by a distance $d_2$, just as discussed in [20]. The results are depicted in figures 5(a)–(d) for different $d_2$: (a) $d_2 = 0.01a$, (b) $0.1a$, (c) $0.3a$, and (d) $0.5a$. It is clearly seen that only two trivial IPMs $\omega_1$ and $\omega_3$ appear. This manifests that a single isolating layer only leads to symmetric or antisymmetric coupling between superlattices I and III. The mode $\omega_2$ never occurs in the present sample. This hints that the origin of the mode $\omega_2$ strongly relies on the coupling among the superlattices and the complex defect structure. On increasing $d_2$, mode $\omega_1$ (mode $\omega_3$) is rapidly shifted upward (downward) to frequency continuum 1 (3) of the bulk plasmons; finally both modes $\omega_1$ and $\omega_3$ are merged into the continua of the bulk plasmons, as seen in figure 5(d) when $d_2$ is greater than $0.5a$.

The dependence of the number of localized IPMs on the number $N$ of barriers in the defect region is displayed in figures 6(a)–(d) for different $N$: (a) $N = 3$, (b) 4, (c) 5, and (d) 6. Here, we choose the same doped electron density $n_1 = n_3 = n_{\mathrm{II},i}$. The period of superlattice III is identical to that of superlattice I, and the width of each layer of the defect structures is $0.1a$. Besides the existence of the trivial modes $\omega_1$ (lower-energy mode) and $\omega_3$ (higher-energy mode), there are other nontrivial IPMs, which are labelled as $\omega_{2a}$, $\omega_{2b}$, $\omega_{2c}$, ..., $\omega_s$, etc. The number of nontrivial IPMs increases with $N$; for instance, it is 1 (see figure 2(a)), 2, 3, 4, and 5 for the numbers of barriers $N = 2$ (see figure 2(a)), 3, 4, 5, and 6, as seen in figures 6(a)–(d). With the increase of the number $N$ of the barriers, the nontrivial mode $\omega_s$ with the highest frequency rapidly approaches the continuum of the bulk plasmons from below this continuum, merges into the continuum, then crosses the continuum and reappears above the continuum with a finite spanning wavenumber range, as seen in figures 6(c) and (d). The nature of this mode $\omega_s$ seems to develop from an acoustic-like mode to an optical-like mode, according to

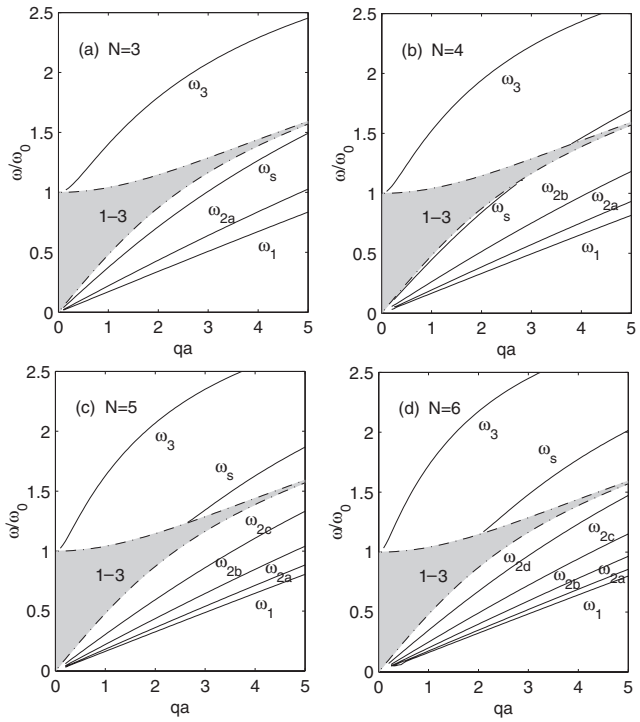


**Figure 6.** The dependence of the number of localized IPMs on the variation of the defect structures. Parts (a)–(d) correspond to the cases where the number $N$ of barrier layers in the defect structures takes the values 3, 4, 5, and 6, respectively. Here, the electron densities in the superlattices I, III and the defect structure II are identical. Other parameters are chosen as $a = b$, and the width of each layer of the defect structures as $0.1a$.

its behaviour in the long-wavelength limit. We conclude that the increase of the number of nontrivial IPMs originates from the coupling of the multiple wells in the defect region.

### *3.2. WBW defect structure*

We now turn to studying a defect structure consisting of a well layer (with an electron density $n_{\mathrm{II},1}$) followed by a barrier (with a width $d$) and a well layer (with an electron density of $n_{\mathrm{II},2}$), in sequence. For convenience, we refer to this as a WBW structure. For matching with the defect structure, we rearrange the sequence of the barrier and well layers in superlattices I and III. The relevant sequence is reversed to the case containing the BWB defect structure. This change of the sequence does not have any influence on the theoretical results for the bulk plasmon modes. That is to say, equations (8$a$) and (8$b$) are still suitable for the current calculations. Equation (8$c$) now is replaced by the following relation:

$$(B\sinh qd + \cosh qd)(C\sinh qd + \cosh qd) = 1. \tag{12}$$

$B$ and $C$ are defined, respectively, as

$$B = \frac{\mathrm{e}^{-\mathrm{i}q_z^{(\mathrm{I})}b}\sinh qb}{r_{\mathrm{II},1}\mathrm{e}^{-\mathrm{i}q_z^{(1)}b}\sinh qb - \frac{\epsilon_1}{\epsilon_2}(1-\mathrm{e}^{-\mathrm{i}q_z^{(1)}b}\cosh qb)},$$

$$C = \frac{\mathrm{e}^{-\mathrm{i}q_z^{(3)}a}\sinh qa}{r_{\mathrm{II},2}\mathrm{e}^{-\mathrm{i}q_z^{(3)}a}\sinh qa - \frac{\epsilon_3}{\epsilon_2}(1-\mathrm{e}^{-\mathrm{i}q_z^{(3)}a}\cosh qa)},$$

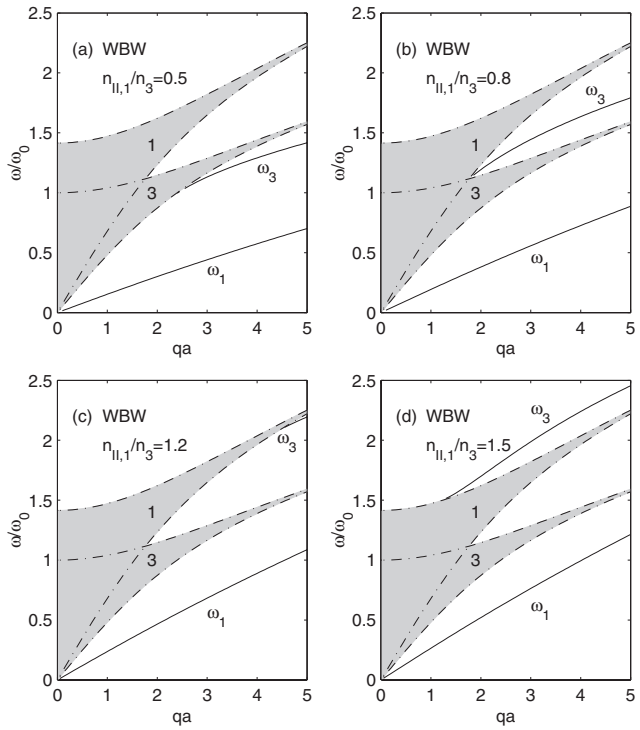


**Figure 7.** The dispersion spectrum of the localized IPMs as a function of the parallel wavenumber $qa$ for different electron densities in the WBW defect structure. We set $n_1/n_3 = 2$, $a = b$, and $d = 0.1a$. The electron densities $n_{\mathrm{II},1}$ and $n_{\mathrm{II},2}$ are identical; their values relative to those of superlattice III are chosen as 0.5, 0.8, 1.2, and 1.5, respectively, corresponding to parts (a)–(d).

where $d$ is the width of the barrier. $r_{\mathrm{II},1}$ and $r_{\mathrm{II},2}$ are respectively associated with the electron densities $n_{\mathrm{II},1}$ and $n_{\mathrm{II},2}$ in the defect structure.

The frequency spectrum of the localized IPMs as a function of the parallel wavenumber $qa$ is shown in figure 7 for different electron densities $n_{\mathrm{II},1}$: (a) $n_{\mathrm{II},1}/n_3 = 0.5$, (b) 0.8, (c) 1.2, and (d) 1.5, respectively. We set $n_1/n_3 = 2.0$, $a = b$, $n_{\mathrm{II},1} = n_{\mathrm{II},2}$, and $d = 0.1a$. The energy continuum bands 1 and 3 are associated with superlattices I and III, respectively. It is observed from figure 7 that there are only two localized IPMs, labelled as $\omega_1$ and $\omega_3$, in contrast to the case of figure 2. The mode $\omega_1$ belongs to the trivial acoustic-like mode with zero frequency when $qa \to 0$; however, the mode $\omega_2$ seems to be an optical-like mode with a finite spanning region of the wavenumbers. On increasing $n_{\mathrm{II},1}/n_3$, the mode $\omega_1$ is gradually shifted upward in frequency, while the mode $\omega_3$ rapidly approaches the lower band edge of continuum 3 and merges into it; across this continuum, this mode reappears between continua 3 and 1; finally, this mode crosses continuum 1 and reappears above continuum 1, as seen in figures 7(a)–(d). Comparing with figures 2, we can conclude that the barrier and the well layers in the defect structures play different roles in the features of the localized IPMs.

## 4. Summary

We have investigated the properties of the localized IPMs in two coupled semi-infinite superlattices caused by complex structural defects consisting of $N$ quantum wells, in detail.

Two types of defect structure are considered: one is a BWB structure; the other is a WBW structure. The numerical results reveal some interesting and novel characteristics of these defect structures. The main findings can be summarized as follows. For the above two cases, the maximal numbers of localized plasmon modes are substantially different. For the BWB structure, three modes are generally produced, in contrast with the existence of only two localized IPMs in the WBW case. This result is associated with the increased splitting of the plasmon modes in the BWB defect structure. Here, the barrier and well layers in the defect structures play different roles in the dispersion behaviour of the localized IPMs. The introduction of each new barrier layer creates an extra localized IPM. So, the more barrier layers the defect structure contains, the greater the number of localized plasmon modes. It is also observed that the actual constitution of the defect structure, the geometric parameters of the constituent layers, and the relative electron density have a substantial influence on the existence, splitting, degeneracy, and evolution of the localized IPMs. It is anticipated that one can artificially engineer the nature of the defect structures, the electron density in the superlattices and in the defect structures, the energy continuum bands, and the localized IPMs to match practical requirements.

## Acknowledgment

This work was supported by the National Science Foundation of China.

## References

[1] Fetter A L 1973 *Ann. Phys.* **81** 367
[2] Olego D, Pinczuk A, Gossard A C and Wiegmann W 1982 *Phys. Rev.* B **25** 7867
[3] Jain J K and Allen P B 1984 *Phys. Rev. Lett.* **54** 947
Jain J K and Allen P B 1985 *Phys. Rev. Lett.* **55** 997
[4] Das Sarma S, Koayashi A and Prange R E 1986 *Phys. Rev. Lett.* **56** 1280
[5] Mayanovic R A and Giuliani G F 1986 *Phys. Rev.* B **33** 8390
[6] Pinczuk A, Lamont M G and Gossard A C 1986 *Phys. Rev. Lett.* **56** 2092
[7] Camley R E and Mills D L 1984 *Phys. Rev.* B **29** 1695
[8] Capasso F, Sirtori C, Faist J, Sivco D L, Chu S N G and Cho A Y 1992 *Nature* **358** 565
[9] Zahler M, Cohen E, Salzman J and Linder E 1993 *Phys. Rev. Lett.* **71** 420
[10] Wang X-H, Gu B-Y, Yang G-Z and Wang J 1998 *Phys. Rev.* B **58** 4629
[11] Gilmore M A and Johnson B L 2001 *Eur. Phys. J.* B **23** 297
[12] El Boudouti E H, Djafari-Rouhani B, Akjouj A and Dobrzynski L 1996 *Phys. Rev.* B **54** 14728
[13] Sedrakyan D G and Sedrakyan A G 1999 *Phys. Rev.* B **60** 10114
[14] Mizuno S 2002 *Phys. Rev.* B **65** 193302
[15] Bah M L, Akjouj A, El Boudouti E H, Djafari-Rouhani B and Dobrzynski L 1995 *J. Phys.: Condens. Matter* **7** 3445
[16] Mendialdua J, Rodriguez A, More M, Akjouj A and Dobrzynski L 1994 *Phys. Rev.* B **50** 14605
[17] Chen K-Q, Wang X-H and Gu B-Y 2002 *Phys. Rev.* B **65** 153305
Chen K-Q, Duan W, Wu J, Gu B-L and Gu B-Y 2002 *J. Phys.: Condens. Matter* **14** 13761
[18] Giuliani G F and Qiunn J J 1983 *Phys. Rev. Lett.* **51** 919
[19] Giuliani G F and Qiunn J J 1984 *Surf. Sci.* **142** 433
[20] Bloss W L 1991 *Phys. Rev.* B **44** 1105
[21] Gu B-Y and Zhang X-L 2002 *Int. J. Nonlinear Sci. Numer. Simul.* **3** 581
[22] Zhang X-L, Gu B-Y and Chen K-Q 2003 *Phys. Lett.* A **316** 107
[23] Bloss W L 1991 *J. Appl. Phys.* **69** 3068
[24] Brazis R, Safonova L and Narkowicz R 1995 *Infrared Phys. Technol.* **36** 51